

RESEARCH

Open Access

Size distribution control of FePt nanocrystals by superhydride

Sara Sadat Parhizgar* and Seyed Ali Sebt

Abstract

FePt nanoparticle systems with high magnetocrystalline anisotropy in $L1_0$ phase are proper candidates for application in magnetic information storage with density more than Gbit/in². FePt nanoparticles are grown by $\text{Pt}(\text{acac})_2$ and $\text{FeCl}_2 \cdot 4\text{H}_2\text{O}$ compounds in phenyl ether solvent using weak reducing agent 1,2-Hexadecandiol ($\text{C}_{16}\text{H}_{34}\text{O}_2$) and strong reducing agent superhydride (LiBEt_3H) in two steps. Structural and magnetic properties of the nanocrystals are studied by XRD, EDS and VSM analysis. Also, the growth mechanism and the effect of double-stage growth on size distribution and the size of FePt nanoparticles are determined. For this purpose, TEM images and EDS results are used. The results show that such growth as "core-shell" leads to form 5-nm, nearly monosized FePt nanoparticles, in which a relative standard deviation is decreased from 18% to 8%.

Keywords: FePt nanoparticle; Size distribution; Reduction method; Superhydride; $L1_0$ structure

PACS: 75. 50. Tt, 75. 75. +a, 75. 50. Ss

Background

Magnetic nanoparticles can increase magnetic memory density to higher than Gbit/in². In this case, one of the basic conditions have high coercive field (H_C), in the Tesla order. It is necessary to make magnetic stability of nanoparticles at room temperature and to overcome the demagnetizing field. To get single-domain magnetic particles with high coercivity, first, metal particles FeCo [1], and barium ferrite [2] in the size order of 0.1 μm were prepared. Magnetic anisotropy in single-domain particles is a combination of magnetocrystalline-, shape- and induced anisotropy [3]. In these particles, the magnetocrystalline anisotropy is small.

The FePt nanoparticles [4] and thin films [5-7] have been made in the last decade. If the nanoparticles are annealed at temperatures above 600°C after a phase transition from face-centered cubic (fcc) to $L1_0$ chemical order face-centered tetragonal (fct) structure, the coercivity increases to Tesla order [8,9]. The high coercivity originating in the FePt nanoparticles after heat treatment is due to the high magnetocrystalline

anisotropy since Fe and Pt atoms are placed separately in parallel lattice planes [10].

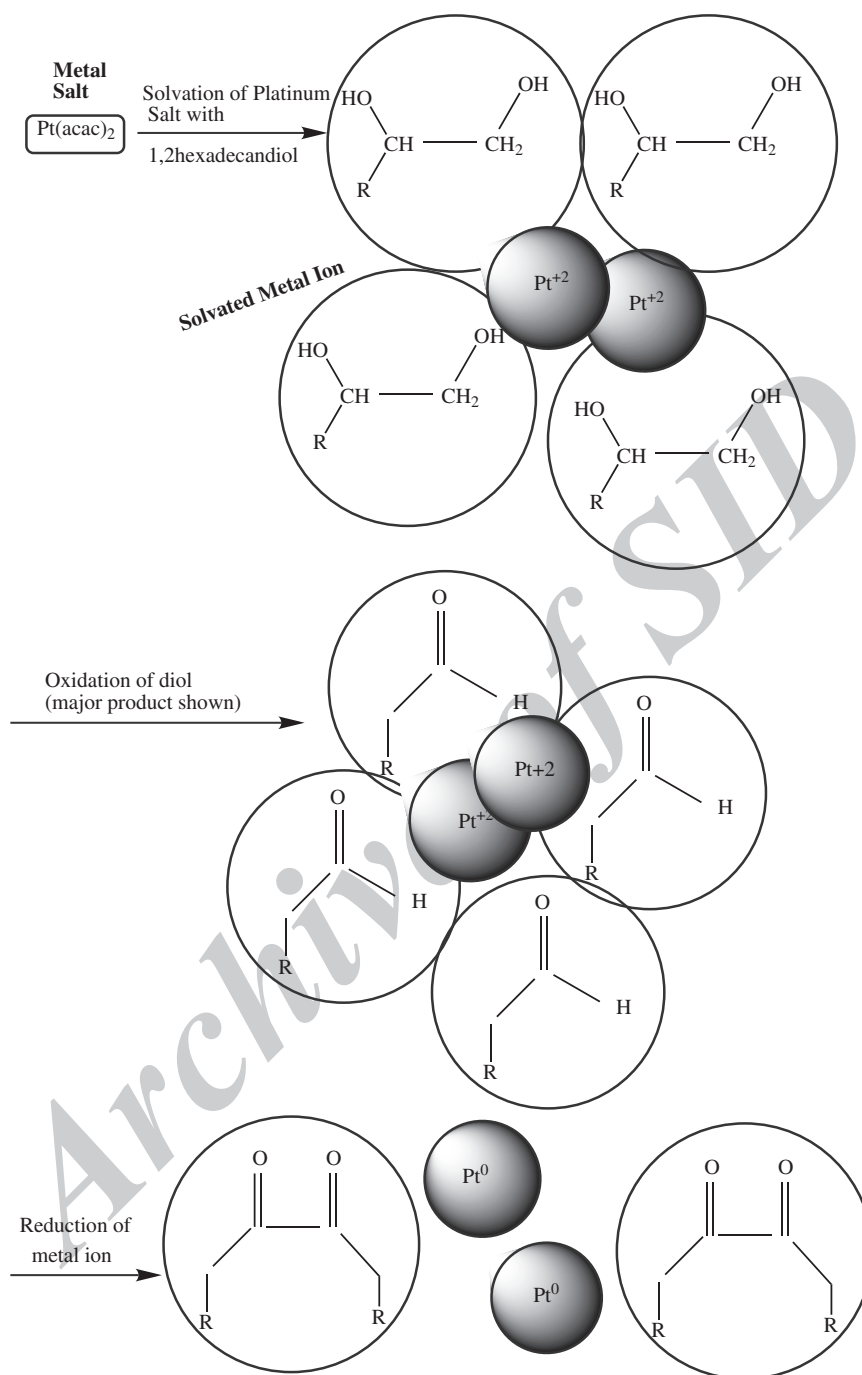
Chemical reduction methods for synthesis of Fe and Pt compositions can lead to single-size FePt nanoparticles [11-14]. Corresponding to the growth rate curve [15], the final size of nanoparticles dependent on monomer concentrations of Fe and Pt in the solvent, and this is because of the reducing agent used and the type of composition and concentration of the precursors. In the present work, samples of $\text{Fe}_{1-x}\text{Pt}_x$ nanoparticles are grown with superhydride (LiBEt_3H) and 1,2-hexadecandiol in two steps, and their magnetic properties and structural analysis are studied via X-ray diffraction (XRD), energy-dispersive X-ray spectroscopy (EDS) and vibrating sample magnetometer (VSM). Also, by TEM images and EDS results, the size distribution of the nanoparticle is determined with discussion by the growth rate curve.

Experimental details

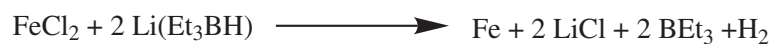
The compositions of $\text{Pt}(\text{acac})_2$ and $\text{FeCl}_2 \cdot 4\text{H}_2\text{O}$ with 1,2-hexadecandiol ($\text{C}_{16}\text{H}_{34}\text{O}_2$) as a poor reducing agent were solved in phenyl ether in nitrogen atmosphere,

* Correspondence: ssparhizgar@gmail.com

Plasma Physics Research Center, Science and Research Branch, Islamic Azad University, P. O. Box: 14665-678, Tehran, Iran



Scheme 1 Procedure of platinum salt reduction by 1,2-hexadecandiol.



Scheme 2 Procedure of iron salt reduction by superhydride.

Table 1 Composition of samples by EDS analysis

Sample	Composition
'a'	Fe ₆₈ Pt ₃₂
'b'	Fe ₆₃ Pt ₃₇
'c'	Pt
'd'	Fe

and the temperature was raised to 100°C in 20 min. Oleic acid and oleylamine were then added and the temperature was raised to 200°C. In this temperature, a strong reducing agent, superhydride (LiBET₃H), was added to the solution which caused a rapid release of metal atoms. After reflux, the system was returned to room temperature.

Scheme 1 illustrates the major product of the platinum salt reduction by 1,2-hexadecanediol [16] and Scheme 2 shows iron salt reduction by superhydride [17].

The concentration of sample 'a' was double compared to that of sample 'b'. For the preparation of samples 'c' and 'd', Pt(acac)₂ and FeCl₂ were used, respectively (Table 1).

Sample purification was done in four stages with centrifuge 8,000 rpm for 10 min. Ethanol and hexane solvents were used in different stages alternately. In the first step, impurities were solved in ethanol and nanoparticles precipitate. The impurities, included residual solvent phenyl ether, suspended solids included BEt₃, and salts which are combination of superhydride Li⁺ cation with Cl⁻ or acac⁻ anions. Then, by adding oleylamine and oleic acid, nanoparticles were suspended in hexane as colloidal solution and after the centrifuge, the remained impurities were deposited.

By transmission electron microscopy (TEM) analysis, with device characteristics (Philips EM 208 TEM (100 kV) 200kX, Amsterdam, The Netherlands), shape, size and size distribution of nanoparticles have been determined. EDS analysis shows the composition of the nanoparticles. Sample 'a' was annealed at 600°C for 4 h under Ar (90%) + H₂ (10%) atmosphere. To distinguish the phase transition after heat treatment, XRD analysis with characteristics (Philips Cu-Kα radiation (λ = 1.54 Å)), and magnetic analysis with device characteristics (model PAR-155), have been performed.

Results

Figure 1 shows the X-ray diffraction of sample 'a' as synthesis and after heat treatment. The peaks in the figure represent the L1₀ structure with chemical order. The appearance of the (001) and (110) peaks in fcc structure shows chemical order, and the splitting of the (200) and (002) peaks show the fcc to fct structure transition with a c/a < 1. In this phase, due to strong crystal anisotropy, FePt nanoparticles become in a ferromagnetic phase with high coercivity.

Figure 2 shows typical magnetic hysteresis loop after annealing at 600°C under Ar (90%) + H₂ (10%) atmosphere, for 4 h. It is evident that coercivity reaches to 0.7 T, which affirms that magnetocrystalline anisotropy has increased. This result is essential for the application of magnetic memory.

Figure 3 shows the TEM images of samples 'a', 'b', 'c', and 'd'. The particles of each two samples 'a' and 'b', are of a single size and are separated. The particle diameter of sample 'a' is approximately two times that of sample 'b' (Figure 3a,b). The platinum nanoparticles in sample 'c' do not have a single size (Figure 3c), but the nano-

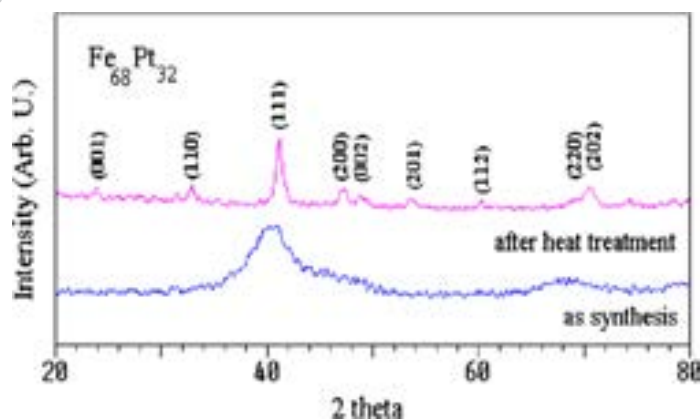


Figure 1 The X-ray diffraction for sample 'a' as synthesis and after heat treatment.

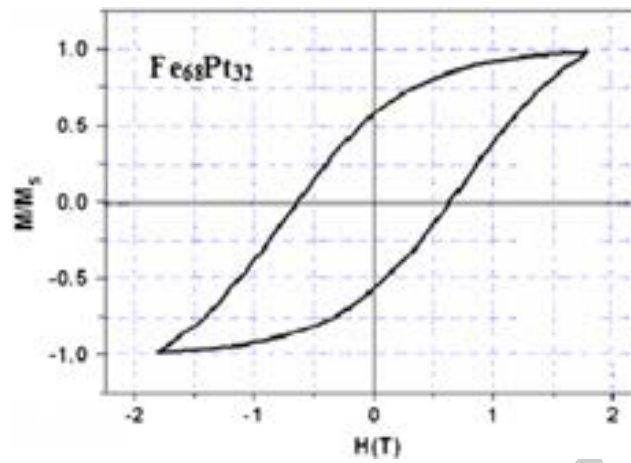


Figure 2 Magnetic hysteresis loop of sample 'a' after thermal process.

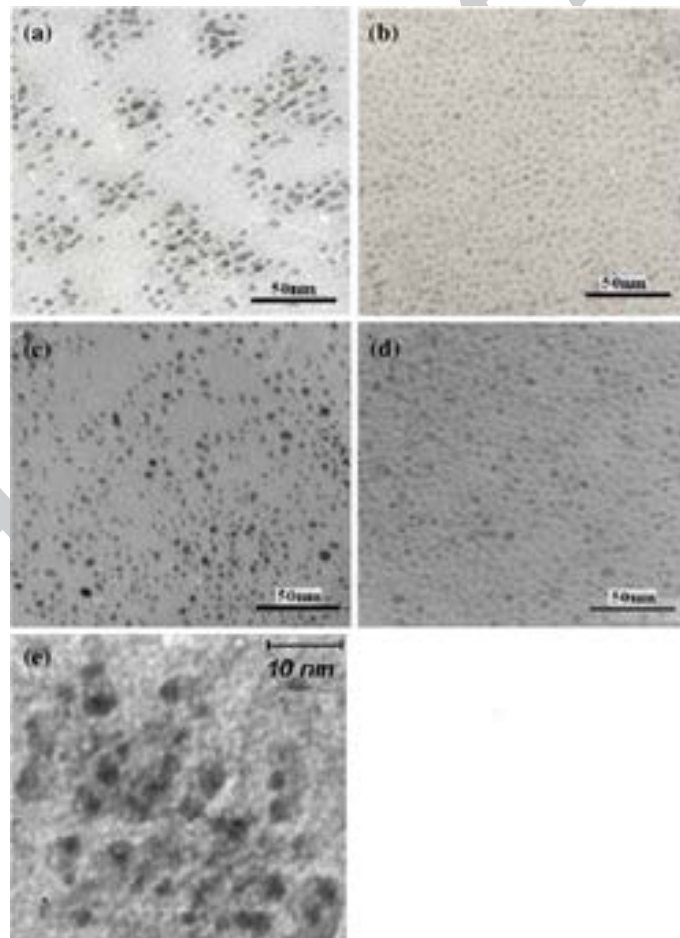
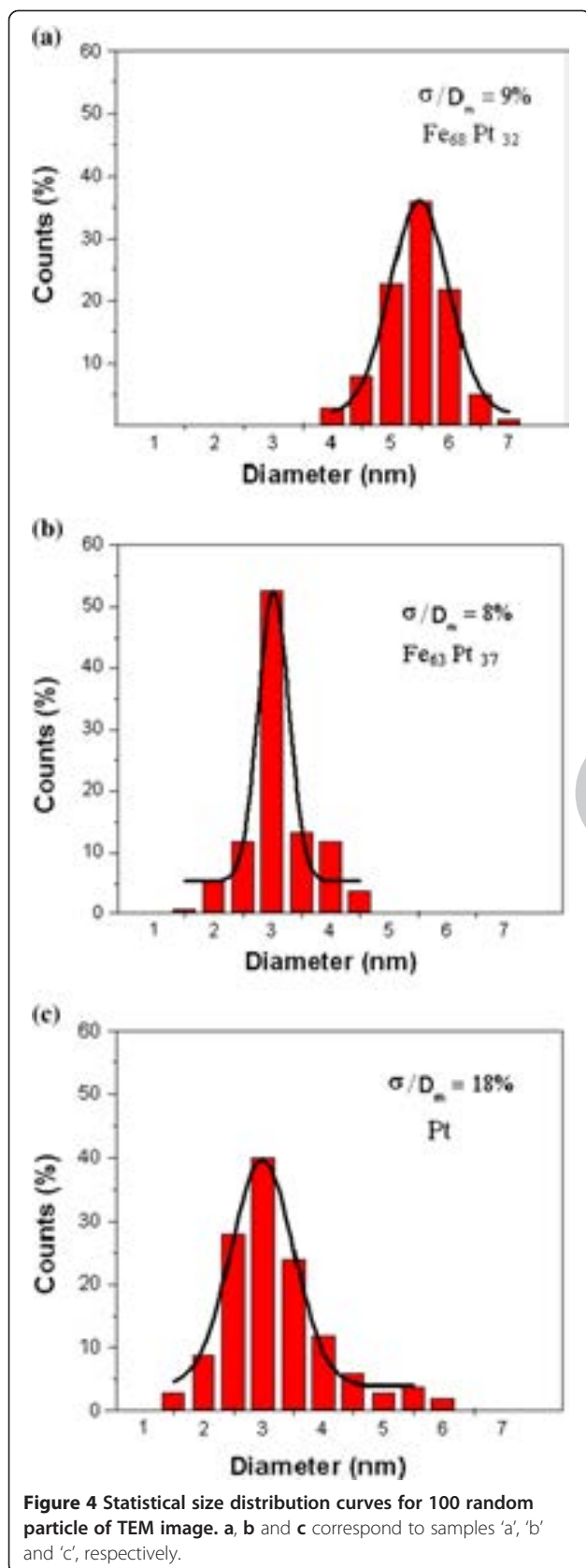


Figure 3 FePt, Pt, and Fe nanoparticles and Pt core and Fe shell structure after reflux. (a,b), TEM images of FePt nanoparticles in two different sizes (samples 'a' and 'b'), (c) Pt nanoparticles with wide statistical size distribution (sample 'c'), (d) Fe nanoparticles and (e) Pt core and Fe shell structure in sample 'a' after reflux.



particles of sample 'd', which are formed by Fe monomers, are almost of a single size and sit close to each other because of the magnetic dipole interactions as shown in Figure 3d. The oleic acid and oleylamine prevent aggregation. Figure 3e shows sample 'a₀' that is extracted from sample 'a' before reflux. In this sample, the core-shell structure is visible. We have shown the ligand effect in separation and stabilization of nanoparticles in [18].

The statistical size distribution diagrams of samples are presented in Figure 4 except for sample 'd'. The hexagonal shape of nanoparticles of sample 'd' and low separation between them caused increasing errors then this curve was eliminated. The average diameter of FePt nanoparticles are 5.5, 3 and 2.3 nm with their relative standard deviation, 9%, 8% and 18%, respectively.

Discussion

The difference between the two samples 'a' and 'b' is in the average diameter of nanoparticles. This is due to the difference in the concentration of monomers in the phenyl ether solvent. In the second stage of growth, the high concentration leads to higher growth rate and larger particle sizes. In the preparation of Fe nanoparticles, FeCl₂ decomposes by superhydride. This reducing agent is so strong that Fe concentration increases rapidly, the smaller seeds grow faster and single-size nanoparticles are created.

The size distribution controlling can be explained as follows: the certain size (critical size, r_c) that the crystals with this size neither grow nor shrink then the smaller nanoparticles are unstable and have negative growth rate. The critical size depends on the monomer concentration, with low monomer concentration favoring a large r_c . After adding a weak reducing agent, the monomer concentration is low then the small nanoparticles are depleted as larger ones grow and size distribution broadens. After adding a strong reducing agent the monomer concentration increases then the critical size shifts to smaller value. In this situation, the smaller nanoparticles grow faster than larger ones because of the geometric factor (increasing the radius of large particles requires the incorporation of more atoms than does increasing radius of smaller particles), and as a result, the size distribution can be focused down to one that is nearly monodisperse [15].

The standard deviation of sample 'c' in size distribution of particles is more than the other three samples. For explanation, one can say that in preparation of sample 'c', where only platinum salt Pt(acac)₂ is used by C₁₆H₃₄O₂ reducing agent, platinum atoms are gradually released. The larger core grows faster because of the low concentration of the Pt atoms. In consequence, Pt

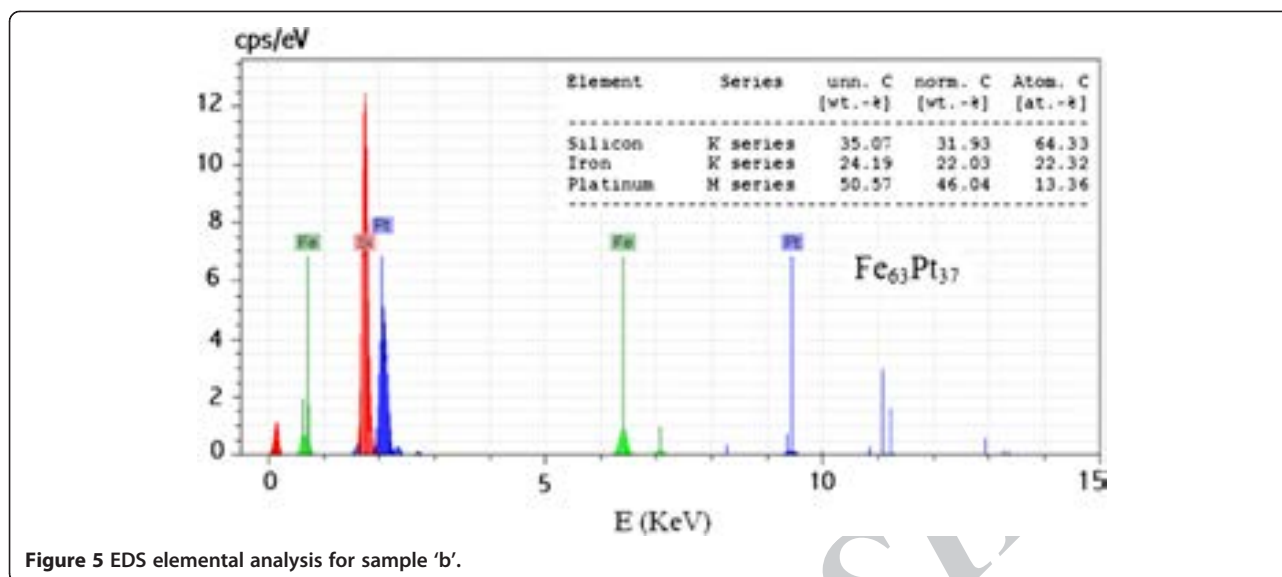


Figure 5 EDS elemental analysis for sample 'b'.

nanoparticles have different sizes and their statistical distribution is wide (Figure 4c).

The growth mechanism of FePt nanoparticles can be explained as follows: First, only the cores are formed by Pt atoms, but iron salt is not reduced by the 1,2-hexadecandiol poor reducing agent. We have been explained that this object in EDS and SEM analysis results in [19]. Then, the reduction accrues immediately after adding superhydride and Fe concentration in the solution rises rapidly. So, suddenly, the critical radius (r_c) reduces in size that almost all of Pt cores which were constructed by the reducing agent $C_{16}H_{34}O_2$ have larger diameter than r_c [15,19]. Therefore, all seeds continue to grow by Fe shells (Figure 3e), but this growth rate is lower for larger particles. Then, the FePt particles are formed in a single size (Figure 3a).

Figure 5 shows the EDS pattern of sample 'b'. The compositions according to the EDS results are observed in Table 1. From Figure 3e and the EDS results of sample 'a₀', one can conclude that the core is composed of Pt and the shell is composed of Fe atoms with lower density.

Conclusions

The Fe, Pt and FePt, nanoparticles are prepared in two stages by the reduction in the presence of two reducing agents: The nucleation stage of nanoparticles by Pt atoms, and shell growth stage with Fe atoms separated by two strong and weak reducing agents. This leads to form single-sized FePt nanoparticles. High concentration of metal ions in shell growth stage increases particle diameters. The size distribution on results of the Fe, Pt

and FePt nanoparticles are discussed by growth rate curve via nanoparticle size. The typical sample average particle diameter is 3 nm with relative standard deviation of 8%.

Competing interests

Both authors declare that they have no competing interests.

Authors' contributions

Both authors, SSP and SAS, carried out the experiments and characterizations, analyzed the data, and conceptualized the research. Both authors read and approved the final manuscript.

Acknowledgements

This work was supported by the office of the Vice-president for Research Science and Research Branch at Islamic Azad University.

Received: 12 February 2013 Accepted: 23 August 2013

Published: 4 September 2013

References

1. Sun, S: Recent advances in chemical synthesis, self-assembly, and applications of FePt nanoparticles. *Adv. Mater.* **18**, 393–403 (2006)
2. Sellmyer, D, Skomski, R (eds.): *Advanced magnetic nanostructures*, p. 187. Springer, Heidelberg (2006)
3. Zoriatstain, S, Azarkharman, F, Sebt, SA, Akhavan, M: Magnetic anisotropies in FeCo fine particles. *J. Magn. Magn. Mater.* **300**, 525–531 (2006)
4. Wang, HB, Wang, H, Zhang, J, Yang, FJ, Xu, YM, Li, Q: Study on composition distribution and ferromagnetism of monodisperse FePt nanoparticles. *Nanoscale Res. Lett.* **5**, 489–493 (2010)
5. Shima, T, Takanashi, K, Takashi, YK, Hono, K, GQ, L, Ishio, S: Nucleation-type magnetization behavior in FePt (001) particulate films. *J. Appl. Phys.* **99**, 033516–033521 (2006)
6. Lai, YC, Chang, YH, Chen, YC, Liang, CH, Chang, WC, Chen, GJ: Inductive magnetization of low-temperature ordered L1₀-FePt with CoAg underlayer. *J. Appl. Phys.* **101**, 053913–053918 (2007)
7. Yang, E, Ratanaphan, S, Zhu, J, Laughlin, DE: Structure and magnetic properties of L1₀-FePt thin films on TiN/RuAl underlayers. *J. Appl. Phys.* **109**, 07B770–07B773 (2011)
8. O'grady, K, Laidler, H: The limits to magnetic recording — media considerations. *J. Magn. Mater.* **200**, 616–633 (1999)

9. Xin-cai, LIU, Ren, XIE, Jing, PAN: Magnetization arrangement of hard magnetic phases and mechanism of magnetization and reversal magnetization of nano-composite magnets. *Trans. Nonferrous Met. Soc. China* **19**, 1131–1145 (2009)
10. Nguyen, HL, Howard, LEM, Stinton, GW, Giblin, SR, Tanner, BK, Terry, I, Hughes, AK, Ross, IM, Serres, A, Evans, JSO: Synthesis of size-controlled fcc and fct FePt nanoparticles. *Chem. Mater.* **18**, 6414–6424 (2006)
11. Christodoulides, JA, Huang, Y, Zhang, Y, Hadjipanayis, GC: CoPt and FePt thin films for high density recording media. *J. Appl. Phys.* **87**, 6938–6941 (2000)
12. Christodoulides, JA, Weller, D: Intrinsic and hysteresis properties of FePt nanoparticles. *Phys. Rev. B* **68**, 054428–054435 (2003)
13. Nandwana, V, Elkins, KE, Poudyal, N, Chaubey, GS, Yano, K, Liu, JP: Size and shape control of monodisperse FePt nanoparticles. *J. Phys. Chem. C* **111**, 4185–4189 (2007)
14. Vázquez, M, Luna, C, Morales, MP, Sanz, R, Serna, CJ, Mijangos, C: Magnetic nanoparticles, synthesis, ordering and properties. *Physica. B* **354**, 71–79 (2004)
15. Yin, Y, Paul Alivisatos, A: Colloidal nanocrystal synthesis and the organic–inorganic interface. *Nature* **437**, 664–670 (2004)
16. Klukovich, HM: Exploration of iron and cobalt core-shell nanoparticles via thermal and microwave polyol synthesis. Dissertation. Wright State University (2006). http://rave.ohiolink.edu/etdc/view?acc_num=wright1162832671
17. Coccoja, M: Nanometallurgy in organic solution: organometallic synthesis of intermetallic transition metal aluminide and –zincide nanoparticles, Dissertation. University of der Ruhr Bochum (2007)
18. Sebt, SA, Parhizgar, SS, Farahmandjou, M, Aberomand, P, Akhavan, M: The role of ligands in the synthesis of FePt nanoparticles. *J. Supercond. Nov. Mgn* **22**, 849–854 (2009)
19. Sebt, SA, Parhizgar, SS: Superhydride effect on formation of single size Pt–Fe core–shell nanoparticles. *Trans. Indian Inst. Met.* (2013). doi:10.1007/s12666-013-0324-0

doi:10.1186/2251-7235-7-44

Cite this article as: Parhizgar and Sebt: Size distribution control of FePt nanocrystals by superhydride. *Journal of Theoretical and Applied Physics* 2013 7:44.

Submit your manuscript to a SpringerOpen[®] journal and benefit from:

- Convenient online submission
- Rigorous peer review
- Immediate publication on acceptance
- Open access: articles freely available online
- High visibility within the field
- Retaining the copyright to your article

Submit your next manuscript at ► springeropen.com